RSC Advances




ROYAL SOCIETY OF CHEMISTRY

www.rsc.org/advances

**Aging behavior of the silicone dielectric elastomers in simulated marine environment**

A. Bele[a], G. Stiubianu[a], S. Vlad[a], C. Tugui[a], C.D. Varganici[a], L. Matricala[a], D. Ionita[a], D. Timpu[a], M. Cazacu[a]

[a] *"Petru Poni" Institute of Macromolecular Chemistry, Aleea Gr. Ghica Voda 41A, 700487 Iasi, Romania*

**Abstract**

A series of silicone-barium titanate composites (multiple specimens of each sample) designed as dielectric elastomeric films to be used as active elements in wave energy conversion devices were immersed in artificial sea water in pseudo-dynamic conditions. While part of specimens were extracted after half a year and subsequently subjected to UV irradiation for 500 h (ASW1/2 + UV procedure), the rest were kept in the saline environment until one year (ASW procedure). The changes occurred in the structure and morphology as well as in mechanical and dielectric properties were assessed by comparing the obtained results to those of the original samples. Thus, the surface and cross-section morphology was studied by Scanning Electron Microscopy (SEM) having attached an Energy Dispersive X-Ray system (EDX), which was used for qualitative elemental analysis and elemental mapping. Changes in surface roughness due to the aging of samples were estimated on the basis of Atomic Force Microscopy (AFM) measurements. The thermal transitions were identified from the Differential Scanning Calorimetry (DSC) data and based on them, the crystallinity degree of the samples were evaluated in each of the three stages. The changes in the structural order were also verified by Wide Angle X Ray Diffraction (WAXD). The tensile toughness, as the amount of energy per volume unit that the material can absorb until failure, was estimated as area under tensile stress-strain curves. The toughness at 100 % elongation was determined on the basis of cyclic stress-strain curves of the original samples as an indirect measure of the energy that the elastic material could release when force that acted on it is removed, like in a harvesting energy system. The aging effect on the viscoelasticity of the samples was evaluated by dynamic mechanical analysis (DMTA), while the dielectric spectroscopy was used to estimate the changes in dielectric properties.

*Keywords*: Polymer-matrix composites, Environmental degradation, Mechanical properties, Electrical properties, Silicones

**1. Introduction**

Silicone rubber is a well-known dielectric elastomer used in electromechanical devices such as actuators or devices for harvesting energy from various natural sources, i.e., human body motion, wind, or ocean waves.[1] Depending on the working and environment conditions, an evaluation of maintenance periods and total lifetime is necessary because degradation processes appear when material is used for long term in outdoor conditions. Therefore, it is important to identify the principal factors involved, so that it can take necessary measures to prevent or delay as much degradation.[2] Silicones can be degraded, mainly at elevated temperatures, in presence of compounds able to act as depolymerisation catalysts.[3] However, the

hydrophobic nature of silicones limits their contact with many aqueous solutions and allows their use in the presence of many chemical compounds. These factors, besides UV transparency confer them outstanding weathering resistance.[4] It has been shown that the main chemical reaction that occurs during aging of silicone rubber is oxidation with formation of by-products of oxidation.[5] Thermal stability of the silicones in general and polydimethylsiloxane (PDMS) in special, either in raw or crosslinked state or containing different additives was studied by a number of research teams both in oxidative and inert atmosphere.[2,6–10] Photo-aging studies on polysiloxanes were also carried out, [2,11–14] either by techniques such as densimetry and hardness measurements[15] or in differential scanning calorimetry (DSC) furnace and the results were discussed in comparison with those obtained by complementary techniques such as thermogravimetrical analysis (TGA) and gel permeation chromatography (GPC)[2]. It has been concluded that both thermal and photo-stability is influenced by the nature of organic substituent at the silicone atom (methyl, vinyl, phenyl, H, etc.).[2] Exposure of silicone rubber to radiation has very similar effects to those caused by heat aging leading to an increase in hardness and a decrease in both tensile and elongation.[16,17]

Marine medium is considered aggressive from chemical (high content of salts), physical (water pressure, wave power, temperature changes) and biological (attachment of bacteria and microalgae) points of view. Although aging in marine environment has been extensively investigated for some organic materials,[18–20] there are few reports about the behavior and aging mechanism of the elastomers such as silicone, in such an environment.[21–24] The processes that can occur in the marine environment are water absorption, hydrolysis, additive extraction, oxidation, in dependence on material nature and composition.[24–26] However, there are very few long term data available, which limits clear explanations of the aging mechanisms involved.[24] Three different silicones formulated to have high refractive index were subjected to accelerated aging tests differing by light source, humidity, temperature, time. The results indicated in general a good survival of the original properties but in dependence on silicone compositions.[27] Other aging tests on the silicone rubber outdoor polymer insulator under salt water based on a standardized procedure (dip wheel, continuous 30 000 test cycles) revealed decreasing in hydrophobicity and increasing in hardness.[28]

In this paper we studied the aging of a series of silicone-barium titanate composites designed to be used as dielectrics in wave energy conversion devices. We have developed these composites in a larger study aiming the optimization of the silicones mainly in terms of mechanical and dielectric properties for use as dielectrics in wave energy harvesting units. We chose barium titanate as filler for silicones, which is one of the most researched dielectric materials, due to its high dielectric permittivity and low loss characteristics. In addition, it can be easily prepared and used, being chemically and mechanically very stable.[29,30] Barium titanate powder of high purity is reported to be a key component in applications, such as energy storage capacitors and multilayer capacitors.[29,31]

Considering the fact that these materials will be an essential part of ocean energy recovery devices that should work as long as possible in a marine environment where, besides water and its components,

sunlight including UV radiation also acts on the immersed materials, we considered appropriate to assess their behavior in such an environment. For this purpose, the composites were immersed for one year in artificial sea water mainly in static conditions with intermittent back and forth movements (ASW procedure). Similar samples extracted after half a year from saline water were further exposed to UV radiation (ASW1/2 + UV procedure). The changes occurred in the morphology, thermal, mechanical and dielectric properties were monitored from time to time. Similar studies have been reported in literature but on other types of composite (i.e., epoxy resins reinforced with glass fiber,[32,33] carbon fiber / epoxy composites[34,35]). We started from the premise that hydrophobic silicone matrix will limit water sorption, which is the key issue in ensuring the long term stability of polymer matrix composites.[34,36,37]

## 2. Experimental

### 2.1. Materials

The polydimethylsiloxane-α,ω-diols, PDMSs, of molecular masses as presented in Table 1 were synthesized according to the already described procedures:[38,39] cationic ring-opening polymerization of octamethylcyclotetrasiloxane in the presence of a cation exchanger as catalyst (PDMS with Mn=40 000 g/mol), and $H_2SO_4$ (for PDMS with Mn 235 000 and 650 000 g/mol). Barium titanate, ($BaTiO_3$), BT, with particle size <3 μm and PLURONIC L-31, HO-poly(ethyleneglycol)-*block*-poly(propyleneglycol)-*block*-poly(ethyleneglycol)-OH (M=1100 g/mol, $d_{25}^{25}$ = 1.02) were purchased from Fluka AG. Methyltriacetoxysilane (MTAS) has been prepared by a procedure adapted from the literature[40] as described in ref.[41] (b.p. =94-97 $^{o}$C, $d_4^{20}$ = 1.17, freezing point - 40 $^{o}$C). The artificial sea water (ASW) used for aging was prepared with distilled water and 3.3 wt% salt from SOLARIS PLANT S.A. without iodine addition.

### 2.2. The procedure for the preparation of PDMS -BT composites

The dielectric silicone composite films were prepared based on components whose amounts are presented in Table 1 and according to procedure described in ref.[42] Thus, pre-established amounts of barium titanate powder were mixed with surfactant PLURONIC L-31. Chloroform (10 ml) was added to obtain a less viscous mixture, which was both mechanically shaken (30 min) and by ultrasound (30 min) and afterwards this mixture was transferred over PDMS. Then, MTAS crosslinker was added and stirred thoroughly until the components formed a homogenous mixture. The resulted mixture was sonicated for 10 minutes in order to remove all the air bubbles trapped and was poured in a Teflon mold (15x5 cm) to obtain films of about 0.5-1 mm thickness. The samples were maintained in air, at room temperature, for 24 h and subsequently the formed films were easily detached from the substrate. The free standing films were then kept in the laboratory environment about one month for aging before characterization by different techniques.

### 2.3. Accelerated aging protocol

The samples, prepared according to the recipes presented in Table 1, were subjected to an accelerated aging process by their immersion in artificial sea water at room temperature and sunlight. Two series containing three pieces of film of each sample were immersed vertically being fixed with staples on pillars existing in artificial sea water bath as in Fig. 1. The bath having immersed samples was subjected from time to time moving back and forth for several hours thus creating a wave-like motion of the water. One of the two series of samples was extracted from this after half a year and further subject to UV irradiation for 500 h (ASW1/2 + UV), while the other was maintained in artificial sea water until one year (ASW).

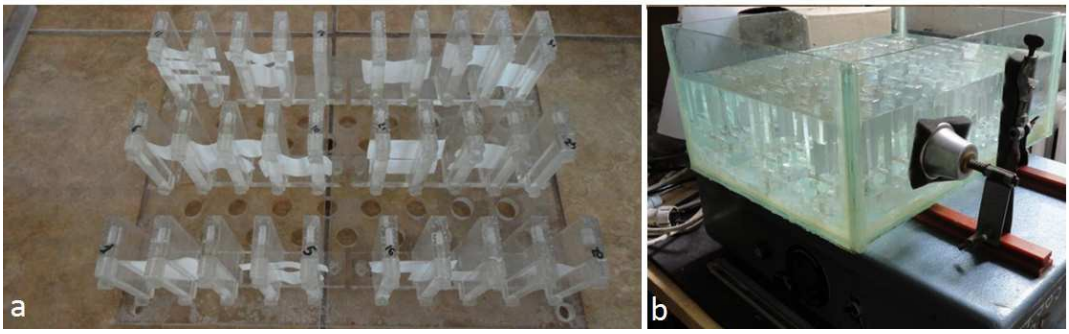


**Fig. 1** Photo of the saline aging bath.

**Table 1** Recipes used for preparation of dielectric elastomeric composites

| Sample | Mn, g/mol | PDMS, g | BT, g | Pl L31, mL | MTAS, g |
|---|---|---|---|---|---|
| M1BT10 | 40000 | 5 | 0.50 | 0.50 | 0.0230 |
| M1BT15 | 40000 | 5 | 0.75 | 0.75 | 0.0230 |
| M2BT10 | 235000 | 5 | 0.50 | 0.50 | 0.0040 |
| M2BT15 | 235000 | 5 | 0.75 | 0.75 | 0.0040 |
| M3BT10 | 650000 | 5 | 0.50 | 0.50 | 0.0015 |
| M3BT15 | 650000 | 5 | 0.75 | 0.75 | 0.0015 |

**2.4. Techniques**

Filler treatment with surfactant and homogenization of the composites before curing were done in a highly intensive ultrasonic bath, Sonoreactor UTR200 (Hielscher Ultrasonics GmbH) with a maximum power density 80 W/cm$^2$, at an amplitude of 60 % and pulse mode ratio 0.5 cycles. UV radiation exposure was

made in a laboratory chamber (Angellantoni Ind., Italy), with a mercury lamp (λ = 200 - 700 nm, incident light intensity of 39 mW $cm^{-2}$), at a temperature of 30 $^{o}$C and humidity of 60%, for a period of 500 h.

**2.4.1. Structural characterization**

FTIR spectra were recorded with a Bruker Vertex 70 FTIR spectrometer in transmission mode on crushed sample by grinding and incorporated into KBr pellets. Raman spectra were recorded in the vibrational frequencies range 100-3250 $cm^{-1}$ by using a Renishaw InVia Reflex spectrometer with a 632.8 nm HeNe laser as excitation source, 10 % power. The laser beam was focused on the film sample and the backscattered Raman signal with a 50x objective lens having a numerical aperture of 0.75 of a Leica DM 2500M microscope. The laser exposure was 10 s. The samples were investigated at low incident laser power in order to avoid sample degradation.

**2.4.2. Bulk crystallization and thermal behavior**

Wide Angle X Ray Diffraction (WAXD) was performed on a Diffractometer D8 ADVANCE (Bruker AXS, Germany), using the Cu-Kα radiation (λ = 0.1541 nm), a parallel beam with Gobel mirror and a Dynamic Scintillation detector. The working conditions were 40 kV and 30 mA, 2s/step, 0.01 degree/step. All the diffractograms were investigated in the range 20-65.2 theta degrees, at room temperature. Differential scanning calorimetry (DSC) measurements were conducted on a DSC 200 F3 Maia device (Netzsch, Germany). A mass of 10 mg of each sample was heated in pierced and sealed aluminum crucibles in nitrogen atmosphere at a flow rate of 50 mL·$min^{-1}$ and a heating rate of 10 $^{o}$C·$min^{-1}$. The temperature against heat flow was recorded. The baseline was obtained by scanning the temperature domain of the experiments with an empty crucible. The instrument was calibrated with indium at various heating rates according to standard procedures.[43]

**2.4.3. Surface characterization**

Scanning electron microscopy (SEM) images were acquired with an electronic microscope type Quanta 200 operating at 30 kV with secondary and backscattering electrons in low or high vacuum mode, while the attached Energy Dispersive X-Ray system (EDX) was used for qualitative analysis and elemental mapping. Atomic Force Microscopy (AFM) images were taken in air, at room temperature, on a SPM SOLVER Pro-M instrument (NT-MDT, Russia). NSG10/Au Silicon tip with a 6 nm radius of curvature, 95 µm cantilever length, force constant: 11.8 N/m and 276 kHz mean frequency oscillation was used. The apparatus was operated in semi-contact mode, 256x256 scan point size, with a scan velocity of 20 ÷ 100 µm/s, (depends on roughness), at different scan areas (foursquare with the side of 50, 20, 10, 5, 3, 1 µm). Nova _1443 soft (for data acquisition) and Image Analysis IA_P9 (for data processing) softs (NT-MDT) were used.

**2.4.4. Mechanical and dielectric characterization**

Stress–strain measurements were performed on TIRA test 2161 apparatus, Maschinenbau GBTH Ravenstein, Germany on dumbbell-shaped cut samples with dimensions of 50x8.5x4 mm. Measurements

were run at an extension rate of 20 mm/min, at room temperature. Cyclic tensile stress tests were performed on the similar samples between 2 and 100 % strain. Five stretch-recovery cycles were registered. The stationary time at minimum and maximum applied stress was 5 s. Dynamic mechanical analysis experiments were carried out on a PerkinElmer Diamond DMA instrument in tension mode on polymeric films with dimensions of 11 mm x 5.2 mm x 0.38 mm. Isochronal measurements were performed over the temperature range -130$^{o}$÷100$^{o}$C using a heating rate of 2$^{o}$C/min and a frequency of 1 Hz. The glass transition temperature values were reported as the maximum in the loss factor peak. Dielectric spectroscopy was performed using the Novocontrol "Concept 40" broadband dielectric spectrometer (Hundsangen, Germany), at room temperature in the frequency domain 1 Hz–1 MHz.

**3. Results and discussions**

Six formulations of PDMS-BT composites differing by molecular weight of the PDMS (Mn 40000, 235000 and 650000) as well as BT content (10 and 15 pph) were prepared (Table 1). After dispersion with surfactant in chloroform medium, BT was incorporated within silicone matrix by mechanical mixing. The homogenized mixtures were processed as films that were stabilized by crosslinking with methyltriacetoxysilane at room temperature according to well-established procedure.[42] The films aged in laboratory conditions were immersed in artificial sea water, part of them for one year (ASW) and another part for half a year. For the second part, the aging procedure was continued in dry state under the influence of UV-Vis radiation (ASW1/2 + UV). Both initial and aged films were analysed by different techniques (FTIR and Raman spectroscopy, WAXD, DSC, SEM, EDX, AFM, mechanical testing, dielectrical spectroscopy,) in order to evaluate the changes produced in their structures and properties as a result of the exposure in the above presented conditions.

**3.1. Structural characterization**

All samples, regardless of the state they are in (non-aging, ASW1/2 + UV or ASW), show very similar FTIR spectra without indicating structural changes. Thus, in all spectra are present bands from about 1020 to 1100 cm$^{-1}$ (Si-O-Si stretch), 800 cm$^{-1}$ ($CH_3$ asymmetric rocking, Si-C asymmetric stretch), 1260 cm$^{-1}$ ($CH_3$ symmetric bending), 2966 cm$^{-1}$ ($CH_3$ asymmetric stretch) and 2920 cm$^{-1}$ ($CH_3$ symmetric stretch).[44] The strong bands around 3400 and 1620 cm$^{-1}$ in some spectra are due to present atmospheric water due to insufficient compaction of the sample in KBr pill. FTIR spectra recorded for three of the composites in the three stages (initial, ASW1/2 + UV or ASW) are demonstrative shown in supporting information as Fig. 1S-3S. In Raman spectra of the samples in the three stages (Fig. 2) there are visible intense bands at 2966 and 2906 cm$^{-1}$ ($CH_3$ asymmetric and symmetric stretch, respectively), 708 and 490 cm$^{-1}$ (Si-O-Si stretch) and very weak bands at 1260 and 1406 cm$^{-1}$ ($CH_3$ symmetric and asymmetric bending, respectively)[44] without significant differences between them. The bands at 187, 226, and 306 cm$^{-1}$ are due to barium titanate.[45] The Raman bands corresponding to the surfactant used, which should occur at around 2975, 2930 and 2875 cm$^{-1}$

overlaps with the peaks corresponding to PDMS, and due to their low intensity, those that should be at 1455, 1350 and 875 $cm^{-1}$ are also not seen in spectra.

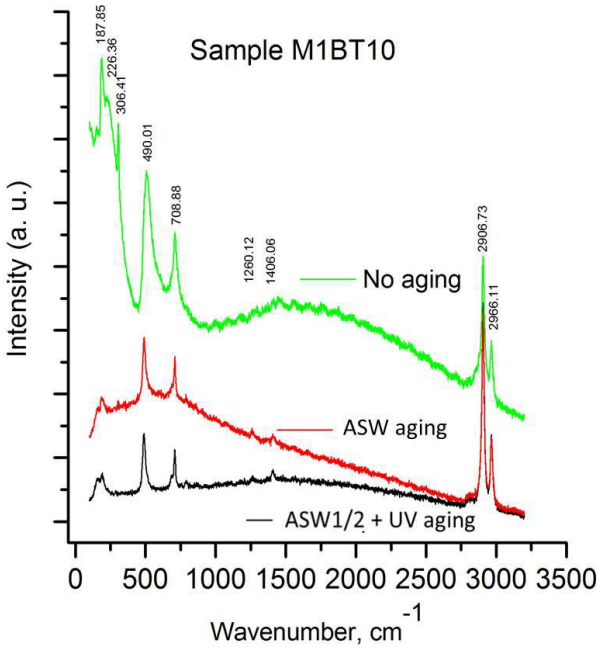


**Fig. 2**. Comparative Raman spectra of the sample M1BT10, original and aged by ASW1/2+UV and ASW procedures.

### 3.2. Changes in bulk crystallization and thermal behavior

X-ray diffraction patterns recorded at room temperature on films for initial samples and those ASW1/2 + UV and ASW aged, respectively, are almost identical (Fig. 3). The diffraction peaks correspond to the barium titanate[45] (Table 1S), silicone matrix being, as is well known, amorphous at room temperature.

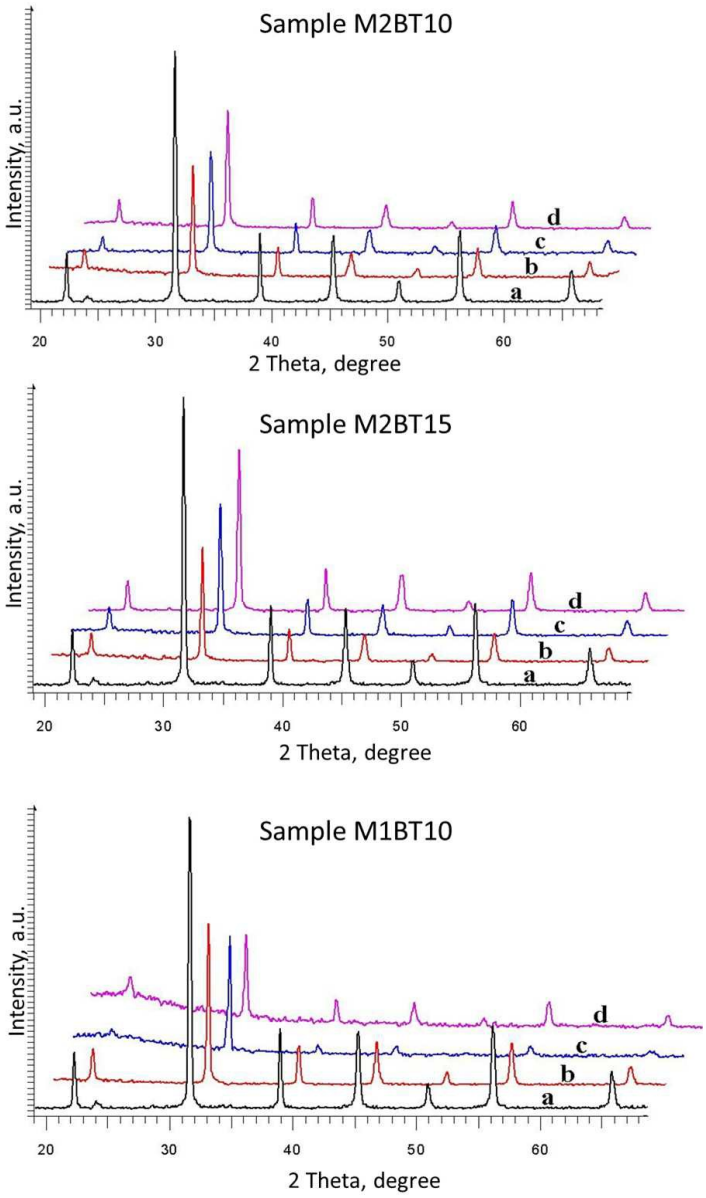


**Fig. 3.** WAXD patterns for: a-barium titanate as compared with composite samples M2BT10, M2BT15 and M1BT10: b – no aged; c – ASW1/2 + UV aged; d – ASW aged.

Differential scaning calorimetry analysis results (Fig. 5S, Table 2S) reveal the glass transition values for the initial samples in the range -123÷ (-120) $^{o}$C. Unsignificant variations occur as a result of aging. However, larger changes are registered for the crystallization degree, $\chi_c$ (Fig. 4), evaluated on the basis of DSC curves (calculated with the equation $\Delta Ht_2/ \Delta H_{literature}$ , where $\Delta H_{literature}$ = 61.3 J $g^{-1}$ [46-50] in dependence on the polymeric matrix structure). As can be observed in Fig. 4, it decreases with decreasing molecular weight of the polymer matrix. This is normal behavior because here the crosslinking degree is higher, thus limiting the

degree of freedom of the chain to adopt ordered conformations. No significant changes develop in the degree of crystallinity of the samples due to variation in the filler content or due to their submission to the two aging processes, excepting M1BT series were a slight decrease in this parameter could be observed after ASW aging.

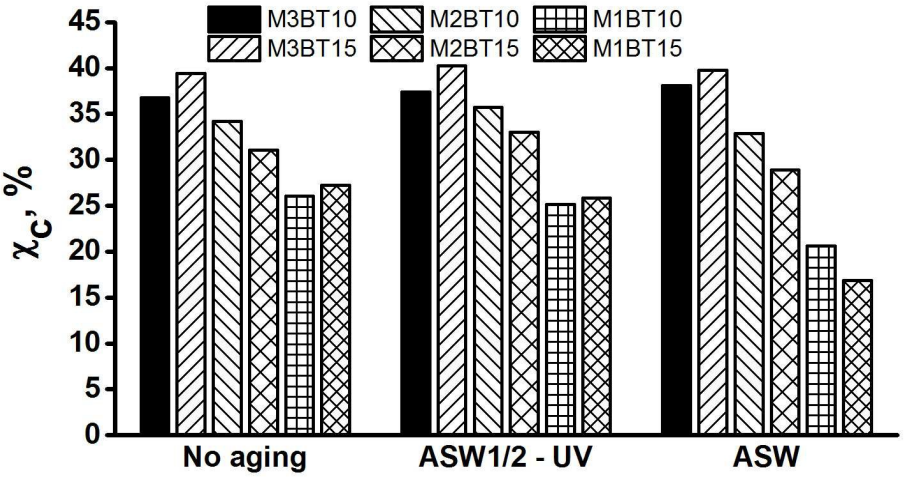


**Fig. 4.** Crystallization degree, $\chi_c$, for M1BT, M2BT, and M3BT series (Table 2S).

### 3.3. Changes in surface morphology

On the SEM images taken on the initial film surfaces, it may be noticed the existence of spherical formations assigned to BT aggregates encapsulated in surfactant, dimensional polydisperse from very small to several microns (Fig. 5a). Islands of surfactant without BT are also visible. After immersion in artificial sea water, half a year and UV irradiation for 500 h, changes occur on the surface of the films. Barium titanate aggregates become more visible besides deposited sodium chloride crystals, while surfactant domains are still present (Fig. 5b). Instead, after one year of stay in artificial sea water, some surface erosion is observed due to the surfactant leaching (Fig. 5c).

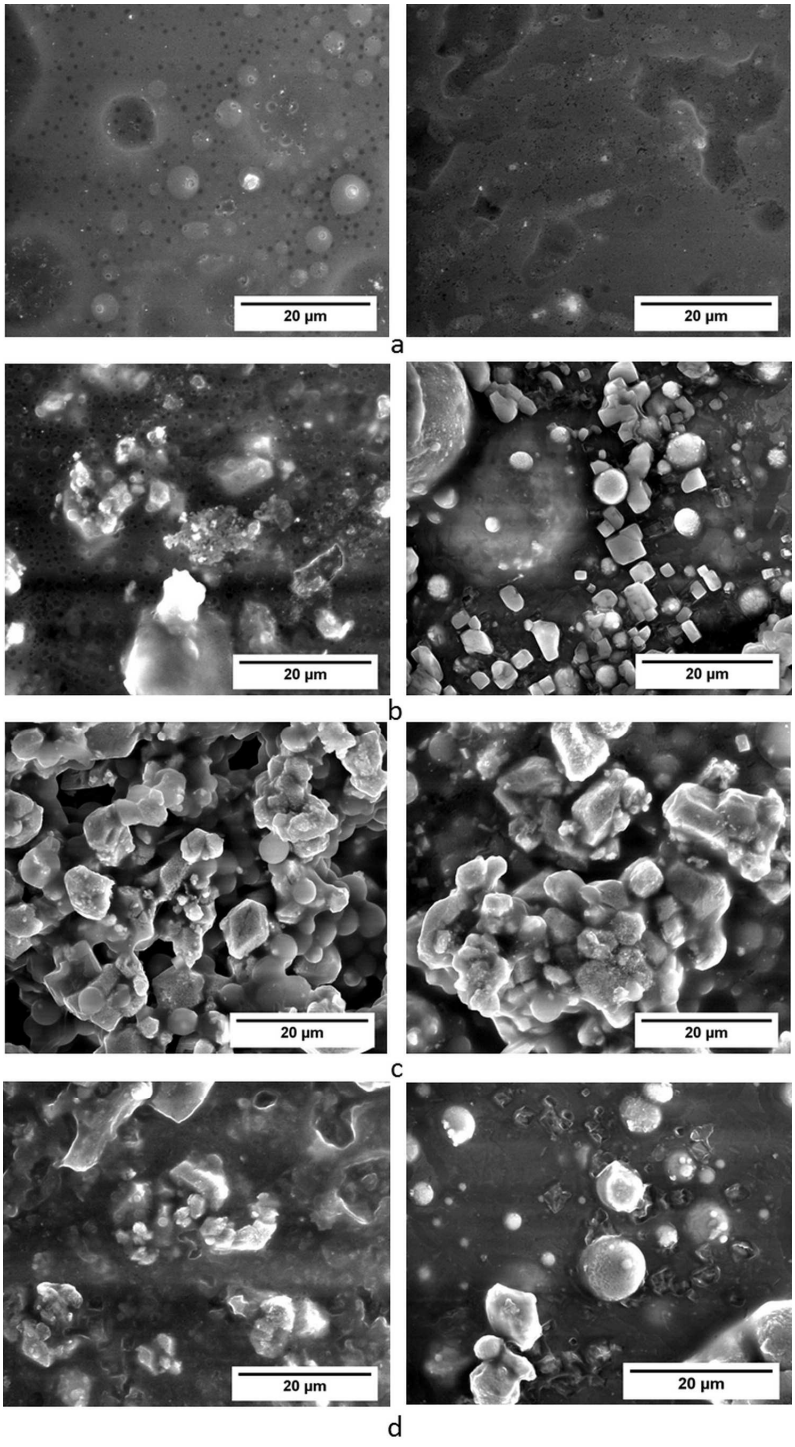


**Fig. 5.** SEM images of M2BT15 (left) and M1BT10 (right) samples in different stages: a – original; b – ASW1/2 + UV aging; c – ASW aging; d – extracted in clean water.

It is presumed that in the high polar medium or/and UV light exposure, the film surface reorganizes leading to considerable increases in its hydrophilicity and roughness as has also been revealed by other studies.[51] AFM images taken on the initial films and those aged through the two procedures after these were well washed with clean water confirm the SEM observations (Fig. 6). The Root Mean Square Roughness, Sq (nm), estimated by statistical processing of the AFM measurements in three different areas with 20x20 µm surface for sample M2BT15, for example, increase from 9.5 (no aged) to 199.6 (ASW1/2+UV) and 346.0 nm (ASW).

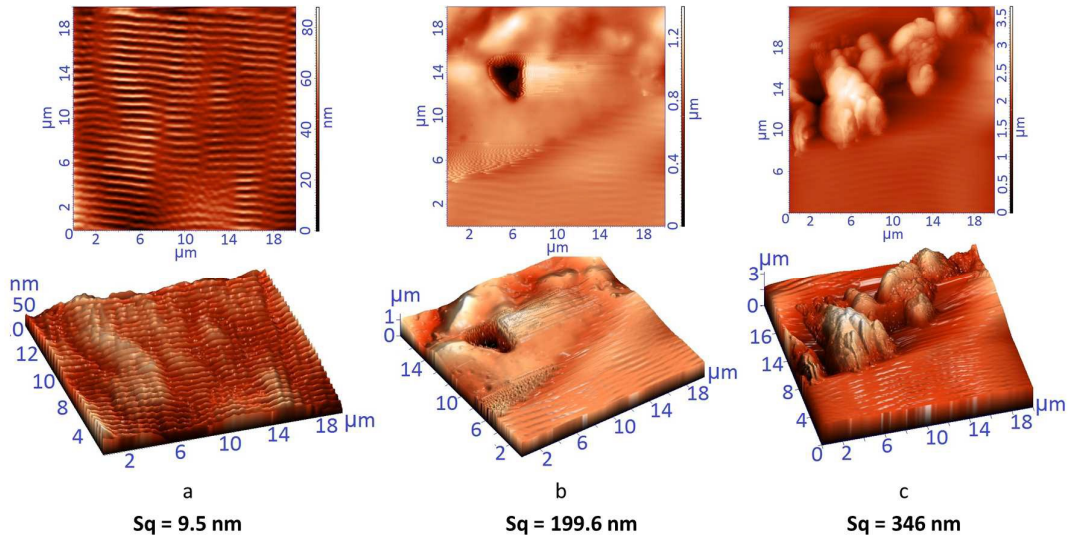


**Fig. 6.** 2D (top) and 3D (down) AFM images for the sample M2BT15: a – no aged; b – ASW1/2 + UV aged, c – ASW aged.

EDX analysis reveals the presence of Na and Cl besides the other expected elements, O, Si, Ba and Ti, on the surface of the aged film (Fig. 7). After extraction with distilled water, one can see the imprint left on the surface film by sodium chloride crystals as track of their dissolution (Fig. 5d). EDX analysis and elemental mapping confirms the absence of Na and Cl on the film surface after washing (Fig. 8). By analyzing again the EDX data of the samples as were removed from artificial sea water (Fig. 7), it can be seen that in samples containing a larger amount of surfactant, such as those of M2BT15 (amount of surfactant incorporated is equal to that of BT as shown in Table 1), a greater amount of chlorine and sodium was found both on surface and in section of the aged films. In the case of sample M2BT10 where a lower amount of surfactant was used, the natrium chloride deposited on the outer surface or migrated into the sample is in very little amount (much below one percent). On this basis, we can opine that the surfactant is one that favors both sodium chloride deposition on the surface and its migration inside the film. Also the amount of natrium and chlorine elements identified by EDAX within the samples increase when the immersion time in artificial sea water is longer.

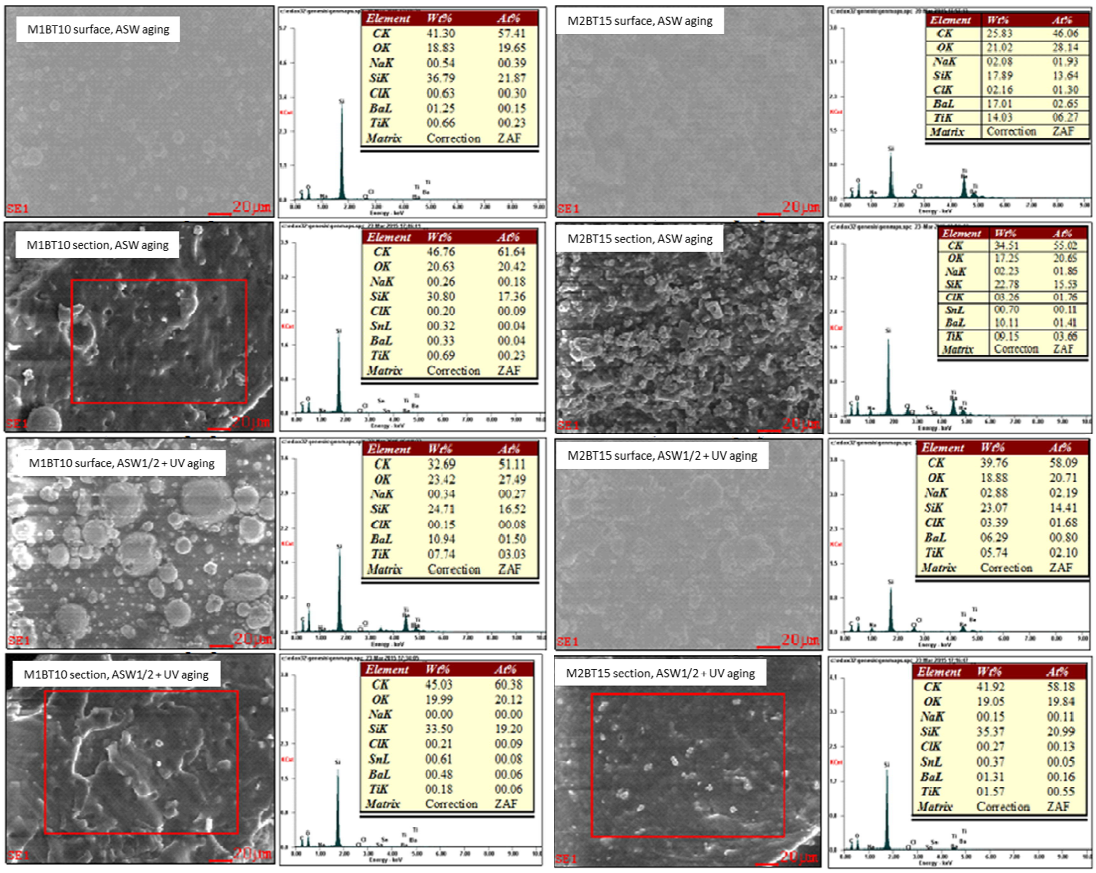


**Fig. 7.** EDX spectra and elemental content estimated for the sample M1BT10 and M2BT15 aged by different protocols, on outer surface and in section.

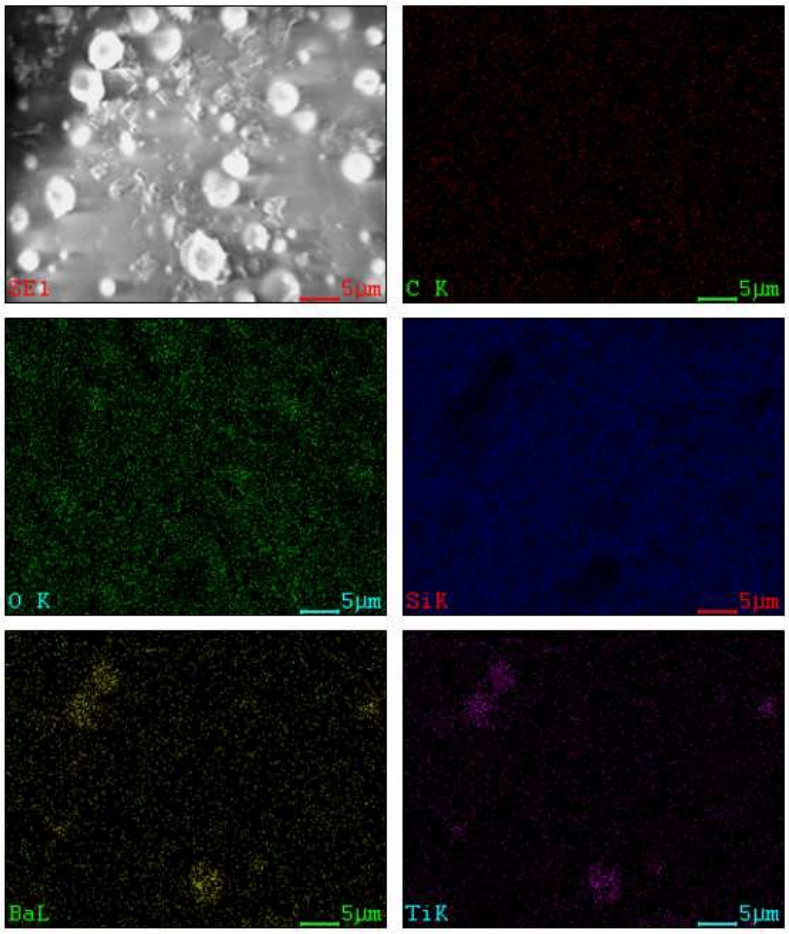


**Fig. 8.** Elements mapping on the surface of sample M1BT10 aged according to ASW1/2 + UV procedure and subsequently washed with clean water.

### 3.4.Changes in mechanical and dielectric behavior

According to literature[52], a modification of the *mechanical properties* of the polymers is to be expected as a result of their marine aging due to water infiltration and degradation of the filler-matrix interface. In the case of silicones, these effects should be less visible due to their known high hydrophobicity. Stress-strain curves of the original samples (Fig. 9a) reveal that the molecular masses along with filler percentage have a great influence on the mechanical behaviour of the composites. Thus, the mechanical strength increases from 0.23 MPa in the M3BT series to 0.41 MPa in the M1BT one, while the maximum strain decreases from 1150 to 151%, respectively (Table 3S, Fig. 10). The difference is greater between the M2BT and M1BT series where molecular mass decreases almost six times, from 235 000 to 40 000. This behavior is expected because the crosslinking density increases as the molecular weight decreases due to the crosslinking performed through chain ends with a trifunctional silane, and the possibility of the chains to slide past each other is reduced. Sample M3BT10, having 10% BT, has a maximum strain of 1150 %. Increasing the amount

of BT at 15 wt%, this drastically decreases to 374 %. In the M2BT series, this decrease is rather moderate one, from 594 % to 455 %, while in the M1BT one there is even a slight increase from 113 to 151 %. The test results for mechanical fatigue resistance, at strains up to 100 % of initial length, show an elastic behaviour in all cases with a clearly visible hysteresis loop only at the first strain-release cycle when the siloxane chains are rearranged in the film and the difference between strain and release was smaller than 1% of the stress value at each point (Fig. 9b). In fact, this behaviour might be associated with Mullins effect (first-cycles stress-softening),[53] which are more visible for the series M3BT based on the highest molecular mass elastomers.

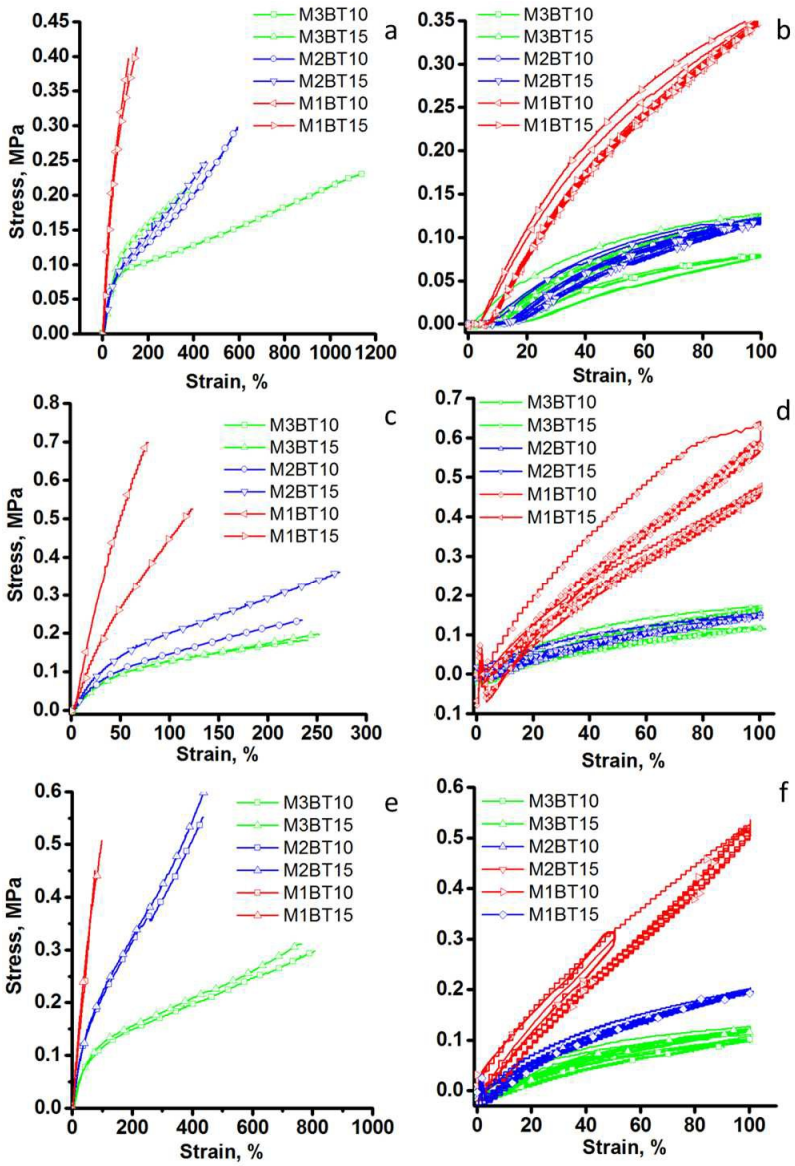


**Fig. 9.** Normal (left) and cyclic (right) stress-strain curves for no aged (a, b), ASW+UV aged (c, d) and ASW aged (e, f) samples.

A drastic decrease of the elongation is observed when the samples were submitted to ASW1/2 + UV aging (Fig. 9c, Table 3S, Fig. 10). It is well-known that silicones are UV resistant, so rises question in connection with other components such as surfactant used. Pluronic L31 is an amphiphile copolymer that acts like a surfactant with the hydrophilic part, poly(ethyleneglycol), oriented to the polar hydrophilic barium titanate particles, while the hydrophobic blocks are oriented in the opposite direction to hydrophobic silicone matrix, thus assuring the compatibilization of the two components and good dispersability of the particles within continue silicone phase. UV degradation of polyethers in general and Pluronic in particular is well documented in the literature [54-58] and it has been shown to result from oxidability of the carbon atoms in the α-position to the oxygen atom.[55] Degradation begins with molecular oxygen addition reaction followed by intermolecular extraction of hydrogen with formation of hydroperoxide species and their foto-induced splitting generating alkoxy radicals. Poly(propyleneoxide) block of Pluronic is more susceptible to degradation due to the high lability of the hydrogen from the tertiary carbon. It is generally agreed that the α-scission of alkoxy radical results in aldehyde carbonyl.[54] Our IR study on the behaviour of surfactant subjected to UV irradiation alone reveals the appearance and development of a new absorption band at 1724 $cm^{-1}$ assigned to formate C=O (Fig. 4S).[54] The weak absorption band at 1641 $cm^{-1}$ could be associated with the bending mode of water molecule in monomer state.[59]

Thus, due to surfactant degradation and its migration outside, the filler is no longer compatible with the matrix and the maximum elongation decrease. The elastic properties are not changed during this aging (Fig. 9d). After one year in saline water only, almost all samples show around 30% decreasing in the maximum elongation values (Fig. 9e, Table 3S, Fig. 10), while the mechanical strength significantly increases, the more the higher molecular weight of the polymer matrix is greater. M3BT and M2BT series still maintain high elongation that suits from this point of view for energy harvesting (more than 400%, up to 800%). The elastic properties are not affected, moreover for M3BT series the hysteresis loop disappears (Fig. 9f).

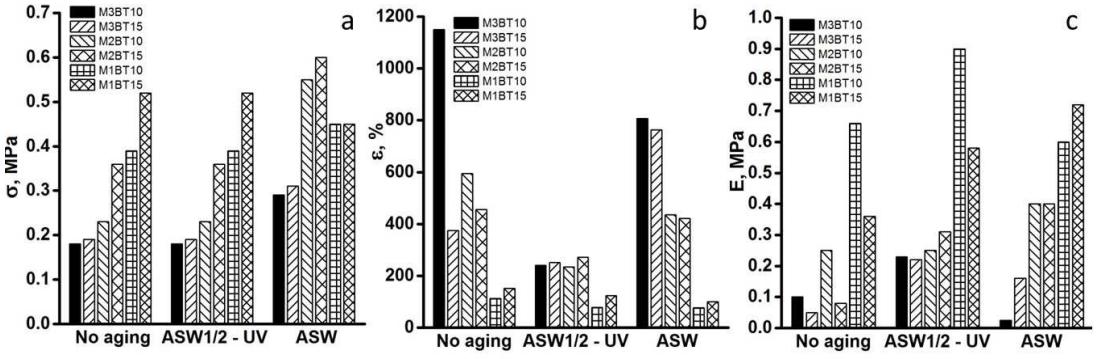


**Fig. 10.** Comparative graphic representation of the relevant mechanical characteristics for all samples in different stages of aging (Table 3S).

The domains characteristic for perfectly elastic materials within the samples behaviour were estimated on the basis of linear part of the stress-strain curves (Table 4S) and the values are graphical showed in Fig. 11 as strain and elasticity modulus values. As expected, elastic modulus increases by decreasing the molecular mass of the polymeric matrix, while the elongation limits slightly decrease. An increasing in elasticity modulus is also registered as a result of either ASW1/2 + UV or ASW aging process, the elongation remaining almost in the same range values.

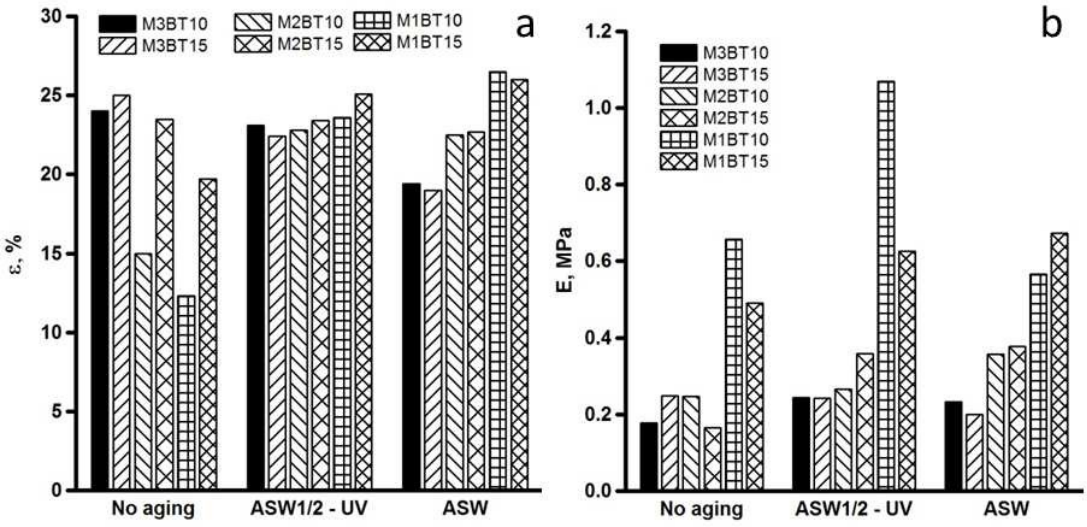


**Fig. 11.** Permanent set values estimated on the basis of tensile tests on the initial samples and after aging (Table 4S).

While the strength indicates how much force the material can support, the tensile toughness is a measure of the amount of energy per volume that a material can absorb to failure and is estimated as area under tensile stress-strain curves (Table 3S).[60-62] The values of the area integrated under the entire stress-strain curve, to the break point, known as ultimate tensile toughness (UTT), are graphically presented for both our original and aged samples in Fig. 12a. As it is known, in order to be tough, a material must be both strong and extensible. If we analyze the entire spectrum of stress-strain curves, and taking into account the structure and composition of the materials, it would be expected as the balance to be best met by the samples based on PDMS having molecular mass of 235000 g/mol (M2BT series). The samples based on the highest molecular mass PDMS (650000 g/mol) (M3BT series) possess low crosslinking density that results in high elongation and low brittleness while the samples from M1BT series, which are based on the lowest molecular mass PDMS (40000 g/mol), are strong but have weak stretching capability. Excepting the original M3BT10 sample, which shows the highest UTT value, 17.46 kJ/m$^3$, this expectation is confirmed. The values for the original M2BT series are larger (9.88 and 6.79 kJ/m$^3$) as compared with the other samples, M3BT15 (5.35 kJ/m$^3$) and M2BT1 series (2.78 and 3.90 kJ/m$^3$). However, these values are lower as compared with those reported in literature for examples, for

stronger polystyrene and ethylene-styrene interpolymers, and estimated on the same bases, when they are ranging between 9 and 61 MJ/m$^3$ in dependence on composition.[62] On silicones, we found in literature the fracture energy estimated for commercial ZruElast™ A1040 to be 6.15 kJ/m$^2$.[63] This suggests that our material would be suitable for harvesting rather low energies. Instead they have the advantage of a good weathering behaviour if properly formulated (e.g., avoid using surfactants). By ASW1/2 + UV aging, significant decrease of the thoughness occurs for the samples M2BT and M3BT (3.06 – 6.11 kJ/m$^3$), while by applying ASW procedure, the values for these samples are significantly higher (13.89-15.53 kJ/m$^3$). An explanation could be that, during the ASW1/2+UV aging process, surfactant through its UV degradation polar products migrates to the outer surface of the non-polar matrix as SEM images revealed (Fig . 5b). Great length of chains between crosslinking nodes of the series M2BT and M3BT and their flexibility facilitates this phenomenon. Proof are and decrease elongation and increasing modulus values for these two series aged by ASW1/2+UV procedure as compared with the values for the initial samples (Fig. 10b , c, Table 3S). The M1BT series having the lowest toughness values seems to be the least affected by the aging process from this point of view.

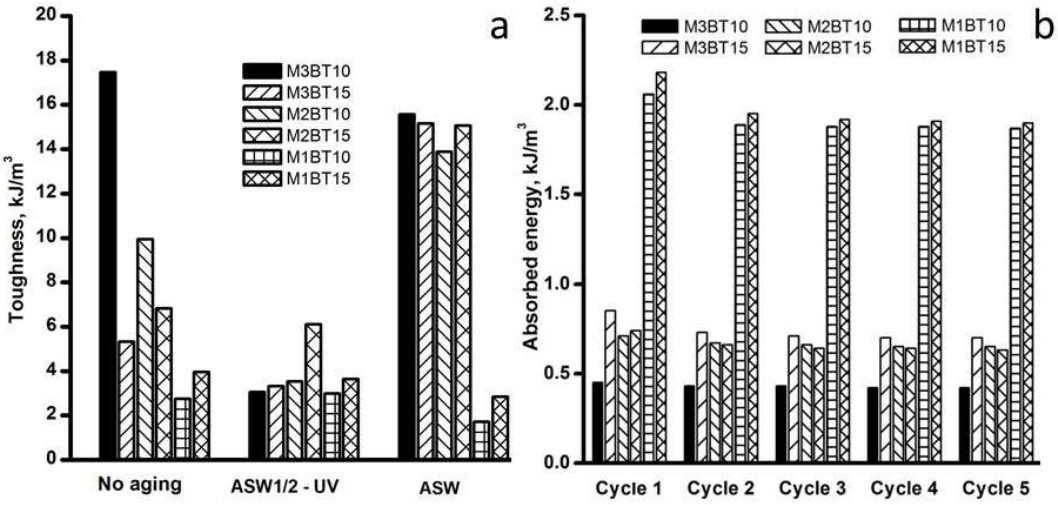


**Fig. 12.** The ultimate tensile toughness (UTT) values in dependence on the aging state for all prepared samples (Table 3S) – a, and toughness at 100 % elongation in cyclic regime for initial samples (Table 5S)– b.

Other values of absorbed energy from an integration of partial stress-strain curves have no standard name. Although it is not a common practice, we evaluated the toughness at 100 % elongation on cyclic stress-strain curves of the original samples as an indirect measure of the energy that the elastic material could release when force that acted on it was removed like in a harvesting energy system. If we analyse the values presented in Table 5S and graphical showed in Fig. 12b, it can see that the M1BT samples show

significantly higher toughness values as compared with M2BTs and M3BTs. Concerning to the effect of the barium titanate content, its enhancing percentage of 5 wt% leads to an increase in toughness with about 3 % in M1BTs but with about 72 % in M3BTs, probably as a result of BT contribution mainly to reduce the extensibility of the sample. Excepting the first cycle, the toughness estimated on the basis of the other cycles is almost unmodified in all cases.

The effect of aging on the viscoelastic properties of M2BT15 sample was also investigated in isochronal measurements using DMTA. Fig. 13 shows in comparison the storage modulus and loss factor spectra for the no aged and aged samples under procedure ASW1/2 + UV and ASW, respectively. Three regions of viscoelastic behavior were observed for all samples: the glassy region, the glass transition region and the rubbery region. The most relevant changes in the viscoelastic behavior brought about by aging on the main viscoelastic characteristic are presented in Fig. 13 and Table 2.

**Table 2**. Viscoelastic characteristics of no aged and aged M2BT15 samples

| Sample | Glassy region | Glass transition region | | Rubbery region |
|---|---|---|---|---|
| | -125 $^{o}$C | | Tg, $^{o}$C | 25 $^{o}$C |
| | E', GPa | tan $\delta_{peak}$ | $h_{tan\,\delta}$ | E'x10$^{-4}$, Pa |
| M2BT15 | 2.5 | -120.8 | 0.085 | 1.71 |
| M2BT15 ASW1/2 + UV aged | 2.6 | -118.7 | 0.088 | 1.73 |
| M2BT15 ASW aged | 2.8 | -119.1 | 0.098 | 4.64 |

$h_{tan\,\delta}$ – the maximum value of tan δ peak

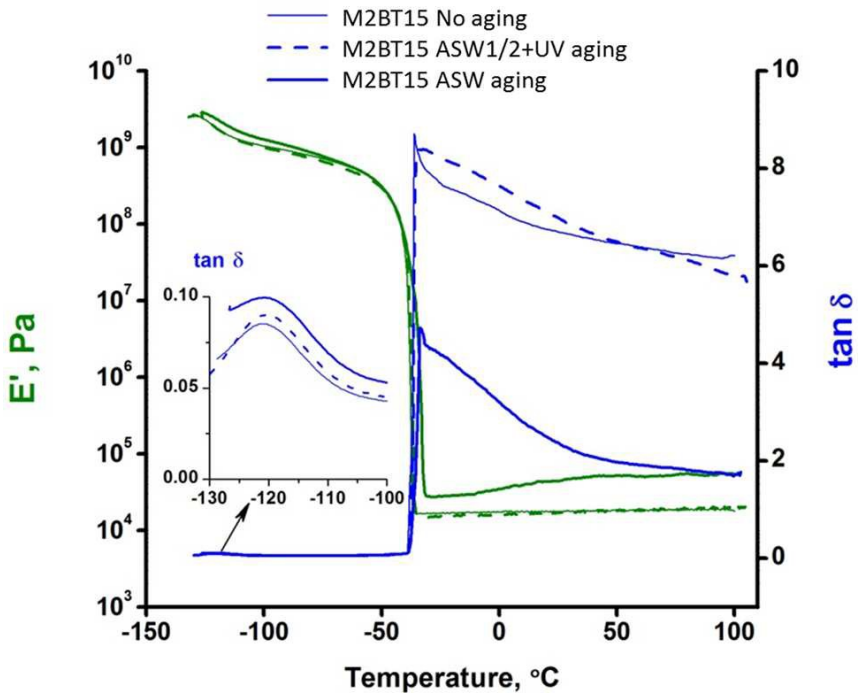


**Fig. 13**. Variation of the storage modulus and loss factor with temperature for no aged and aged M2BT15 samples

The glassy region was characterized by a stiff material response evidenced by a storage modulus higher than $10^9$ Pa. In this region, the macromolecular chains are in frozen state, so the segmental mobility is restricted. An increase in E' is observed after aging, either by ASW1/2 + UV or ASW procedure reflecting a higher rigidity. This trend is similar to those recorded for the evolution of Young's modulus. The aging also modifies the viscoelastic behavior in the glass transition region. The beginning of α-relaxation associated with the glass transition of M2BT15 is marked by a gentle drop in the storage modulus and is accompanied by a small tan δ peak. The very low value of tan δ and the decrease of E' with less than one order of magnitude are justified by the presence of crystalline domains in PDMS as was already proved by DCS measurements. These crystalline regions act as crosslinking points and restrict the long range segmental motion characteristic to a glass transition, thus providing the prevailing of the elastic component over the viscous component. After aging, the onset of E' drop and the tan δ peak are shifted slightly to higher temperatures compared with the sample before aging, resulting in a slight increase in Tg. Interestingly, the aging also generates an increase in intensity and a broadening of tan δ peak (left side inset of Fig. 13). The broadening of the tan δ peak indicates the presence of a more heterogeneous structure, whereas the increase in amplitude reflects a higher mobility of polymeric chains. As the temperature is raised above Tg, an abrupt decrease of the storage modulus accompanied by a sharp change in tan δ was observed. These changes mark the melting of the crystalline phase, which comes out at the same temperature (-49 $^{o}$C) for all samples. After the sharp drop, the storage modulus of the non-aged and ASW1/2 + UV aged reaches plateaus at a

relatively constant value (around $10^4$ Pa) and preserves a good thermal stability until the end of the experiment. The increase of temperature above -40 $^oC$ brings additional rigidity for M2BT15 ASW aged. Therefore an increase in E' is observed in this region strongly dependent on the chemical structure of the polymer.

As expected, the *dielectric permittivity* for samples without aging increases by incorporation of barium titanate, a dielectric ceramic. Thus, while pure crosslinked PDMS have ε'~3 at 10 Hz, increases up to 4.95 and 5.89 for M3 series, 4.41 and 5.07 for M2 series, 3.78 and 5.03 for M1 series was observed. Comparing the samples containing the same amount of BT, we can conclude that even the polymeric matrix has a contribution, from 3.78 up to 4.95 for samples with 10% BT (Fig. 14a, Table 3S). There is a sudden drop at about $10^3$ Hz for ε`, accompanied with the maximum dielectric loss, ε" (Fig. 14b), suggesting a relaxation process occurring at silicone-filler interface. The decrease in the dielectric permittivity is due to the inability of the dipoles to return to its original random orientation, known as relaxation time, which is larger than the rate of oscillating electric field.

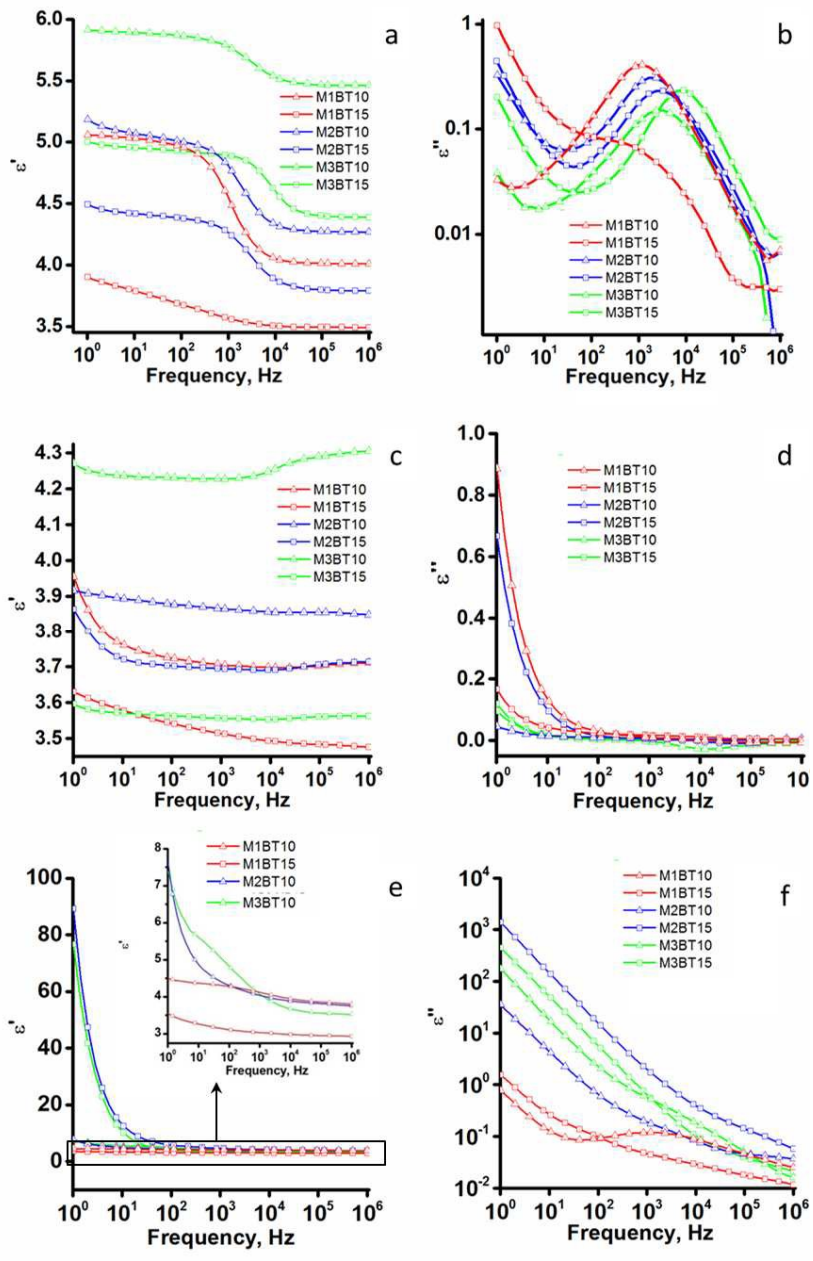


**Fig. 14.** Frequency variation of dielectric permittivity (left) and dielectric losses (right) for samples without aging (a, b), after ASW1/2+UV aging (c, d) and ASW aging (e, f).

After ASW1/2+UV aging (Fig. 14c, d, Table 3S), slight decreases in dielectric permittivity and dielectric loss are observed and, moreover, stabilization at high frequencies occurs. After one year in saline water (ASW) along with an increase in permittivity, a high increase in dielectric loss was observed for M3BT and M2BT series (Fig. 14e, f, Table 3S), due to the salt ions that migrate inside films as EDX results showed (Fig. 7). For M1BT series, a small decrease both in dielectric permittivity and dielectric loss can be noticed. However, the

conductivity-frequency curves (Fig. 6S) show that all samples are maintained in semiconductor ($10^{-18}$ - $10^{-8}$ S/cm) field regardless of the aging process in which they were submitted.

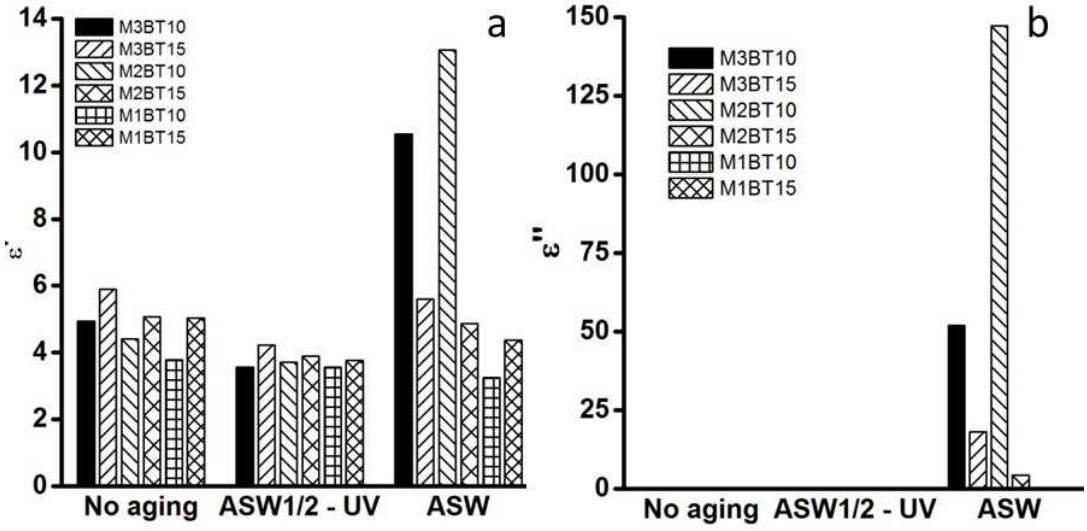


**Fig. 15.** Comparative dielectric permittivity and loss values at 10 Hz for all samples in different stages of aging (Table 3S).

Analyzing the results from the perspective of the target application of the prepared materials, e.g., their use as active elements in devices for wave energy harvesting, it can be said that, the main features that determines the electromechanical functionality are Young modulus that must be kept low, high elongation, high dielectric permittivity and low dielectric loss but also their constancy for a longer period in the given conditions (immersed in seawater under the influence of sunlight, which includes UV radiation). Considering the molecular weight of PDMS matrix and content of BT including compatibilizing agent (surfactant) as control parameters for their design, based on the mechanical and dielectric measurements results, it can be appreciated that increasing molecular weight leads, as it expected, to lower modulus and increased elongation. The BT and surfactant addition in increasing amounts has the effect of increasing the dielectric permittivity up to 33% for 5 wt % addition of BT but both elongation and modulus decrease. Dielectric loss amounts are low and do not vary significantly. As a result of the successive action of salt water and UV ( ASW1/2+UV), dielectric permittivity and the elongation decreased significantly and the modulus increases, while the prolonged action of salt water only (ASW) does increase all these parameters, elongation, modulus, but the dielectric permittivity and loss. Some anomalies in the behavior of composites, such as lowering modulus when increases the BT addition, but also different aging patterns in the conditions ASW1/2+UV or ASW only are determined by surfactant that can play and lubricant role but is photodegradability is the weak point of the composite formula.

**4. Conclusions**

Six silicone composite samples differing by the molecular masses of the matrix polymers as well as by the content of barium titanate incorporated were crosslinked by condensation with methyltriacetoxysilane in form of films. These were aged either by immersion in artificial sea water for half a year followed by UV irradiation for 500 h (ASW1/2 + UV) or one year only in salt water without irradiation (ASW). A slight erosion of the surface occurred as a result of these treatment regimes due both to the physical organization of the hydrophobic siloxane chains and to the surfactant degradation and migration. The surface roughness significantly increases due to the aging as was estimated by AFM measurements. The mechanical characteristics are significantly affected when ASW1/2 + UV aging was applied, while the dielectric permittivity is mainly affected by a longer exposure to sea water only (ASW). Although the analyses by FTIR and Raman spectroscopies as well as by WAXD not evidenced structural changes of the composites as a result of their exposure in established conditions, it seems that the presence of surfactant used for dispersing the filler in the polymer matrix has negative effects on the aging process favoring the deposition of salt on the surface of the film and even migration inside it. The crystallinity degree as estimated on the basis of DSC measurements is influenced by the chain length and not the filler content nor the aging process on which the sample was subjected. The tensile toughness values determined from cyclic stress-strain curves elongated up to 100% suggests a greater capacity to harvest energy for the original samples based on the lower molecular weight polymer. However, the aging brought slight changes in the viscoelastic behavior reflecting in increased storage modulus as well as in Young modulus values. Although ranges for dielectric permittivity and losses in dependence on the frequency do not change significantly, their patterns are different when the initial samples and those aged through ASW1/2+UV and ASW procedures are compared.

**Acknowledgements**: The work presented in this paper is developed in the context of the project PolyWEC (www.polywec.org, prj. ref. 309139), a FET-Energy project that is partially funded by the 7th Framework Programme of European Community and co-financed by Romanian National Authority for Scientific Research, CNCS-UEFISCDI (Contract 205EU). Thanks dr. Iuliana Spiridon who allowed us access to UV irradiation aging chamber, and dr. Elena-Laura Ursu for recording Raman spectra.

**Notes and references**

1 N. Gharavi, M. Razzaghi-Kashani and N. Golshan-Ebrahimi, *Smart Mater. Struct.*, 2010, **19**, 025002.

2 N. S. Tomer, *Open J. Org. Polym. Mater.*, 2012, **02**, 13–22.

3 T. Tadros, *Encyclopedia of Colloid and Interface Science*, Springer, Wokingham, Berkshire, 2013.

4 A. Colas, *Silicones: Preparation, Properties and Performances,*Dow Corning Life Sci., 2005, 1-14.

5 B. H. Chudnovsky, *Electrical Power Transmission and Distribution: Aging and Life Extension Techniques*, CRC Press, 2012.

6 N. Grassie, K.F. Francey and I. G. Macfarlane, *Polym. Degrad. Stab.*, 1980, **2**, 67–83.

7 C. Camino, S. M. Lomakin and M. Lazzari, *Polymer*, 2001, **42**, 2395–2402.

8 G. Camino, S. M. Lomakin and M. Lageard, *Polymer*, 2002, **43**, 2011–2015.

9 E. Vallés, C. Sarmoria, M. Villar, M. Lazzari and O. Chiantore, *Polym. Degrad. Stab.*, 2000, **69**, 67–71.

10 T. H. Thomas and T. C. Kendrick, *J. Polym. Sci. Part -2 Polym. Phys.*, 1969, **7**, 537–549.

11 Y. Israeli, J. Lacoste, J. Cavezzan and J. Lemaire, *Polym. Degrad. Stab.*, 1995, **47**, 357–362.

12 Y. Israeli, J.-L. Philippart, J. Cavezzan, J. Lacoste and J. Lemaire, *Polym. Degrad. Stab.*, 1992, **36**, 179–185.

13 Y. Israëli, J. Cavezzan and J. Lacoste, *Polym. Degrad. Stab.*, 1992, **37**, 201–208.

14 Y. Israëli, J. Lacoste, J. Cavezzan and J. Lemaire, *Polym. Degrad. Stab.*, 1993, **42**, 267–279.

15 F. Virlogeux, D. Bianchini, F. Delor-Jestin, M. Baba and J. Lacoste, *Polym. Int.*, 2004, **53**, 163–168.

16 K.-C. Cheng, C.-M. Lin, S.-F. Wang, S.-T. Lin and C.-F. Yang, *Mater. Lett.*, 2007, **61**, 757–760.

17 P. J. Flory and J. Rehner, *J. Chem. Phys.*, 1943, **11**, 521.

18 N. Guermazi, K. Elleuch and H. F. Ayedi, *Mater. Des.*, 2009, **30**, 2006–2010.

19 E. Legghe, E. Aragon, L. Bélec, A. Margaillan and D. Melot, *Prog. Org. Coat.*, 2009, **66**, 276–280.

20 J. Unsworth and Y. S. Ng, *Internationnal conference on Polymers in a marine environments,* 1984, **97**, 73-76.

21 K. Ab-Malek and A. Stevenson, *J. Mater. Sci.*, 1986, **21**, 147–154.

22 D. Oldfield and T. Symes, *Polym. Test.*, 1996, **15**, 115–128.

23 M. Rutkowska, K. Krasowska, A. Heimowska, I. Steinka and H. Janik, *Polym. Degrad. Stab.*, 2002, **76**, 233–239.

24 P. Y. Le Gac, V. Le Saux, M. Paris and Y. Marco, *Polym. Degrad. Stab.*, 2012, **97**, 288–296.

25 I. Merdas, F. Thominette and J. Verdu, *Polym. Degrad. Stab.*, 2003, **79**, 419–425.

26 P. H. Mott and C. M. Roland, *Rubber Chem. Technol.*, 2001, **74**, 79–88.

27 K. R. McIntosh, N. E. Powell, A. W. Norris, J. N. Cotsell and B. M. Ketola, *Prog. Photovolt. Res. Appl.*, 2011, **19**, 294–300.

28 Y. X. Zhou, Q. Nie, Z. Z. Chen and R. Liu, *J. Phys. Conf. Ser.*, 2009, **183**, 012013.

29 M. M. Vijatović, J. D. Bobić and B. D. Stajanovic, *Sci. Sinter.*, 2008, **40**, 155–165.

30 F. Jona G. Shirane, *Ferroelectric Crystals*, Dover Publications, New York, 1993.

31 P. Kim, S. C. Jones, P. J. Hotchkiss, J. N. Haddock, B. Kippelen, S. R. Marder and J. W. Perry, *Adv. Mater.*, 2007, **19**, 1001–1005.

32 D. Miller, J. F. Mandell, D. D. Samborsky and B. A. Hernandez-Sanchez, *Performance of Composite Materials Subjected to Salt Water Environments*, Honolulu, Hawaii, 2012, 23–26.

33 A. Boisseau, P. Davies and F. Thiebaud, *Appl. Compos. Mater.*, 2011, **19**, 459–473.

34 G. Sala, *Compos. Part B Eng.*, 2000, **31**, 357–373.

35 I. F. Soykok, O. Sayman and A. Pasinli, *Compos. Part B Eng.*, 2013, **54**, 59–70.

36 P. Musto, M. Galizia, G. Scherillo and G. Mensitieri, *Durability of Composites in a Marine environment,* 2014, **208**, 15-45.

37 S. Samaržija-Jovanović, V. Jovanović, G. Marković, S. Konstantinović and M. Marinović-Cincović, *Compos. Part B Eng.*, 2011, **42**, 1244–1250.

38 M. Cazacu and M. Marcu, *J. Macromol. Sci. Part A*, 1995, **32**, 1019–1029.

39 M. Cazacu, C. Racles, A. Vlad, M. Antohe and N. Forna, *J. Compos. Mater.*, 2009, **43**, 2045–2055.

40 W. Noll, *Chemistry and technology of silicones*, Academic Press, New York and London, 1968.

41 A. Bele, M. Cazacu, G. Stiubianu and S. Vlad, *RSC Adv.*, 2014, **4**, 58522–58529.

42 A. Bele, M. Cazacu, G. Stiubianu, S. Vlad and M. Ignat, *Compos. Part B Eng.*, 2015, **68**, 237–245.

43 G. W. H. Höhne, H. K. Cammenga, W. Eysel, E. Gmelin and W. Hemminger, *Thermochim. Acta*, 1990, **160**, 1–12.

44 D. Cai, A. Neyer, R. Kuckuk and H. M. Heise, *J. Mol. Struct.*, 2010, **976**, 274–281.

45 Z. Lazarevic, N. Romcevic, M. Vijatovic, N. Paunovic, M. Romcevic, B. Stojanovic and Z. D. Mitrovici, Acta Phys. Pol., A, 2009, **115**, 808–810.

46 C. M. Roland and Ca. Aronson, *Polym. Bull.*, 2000, **45**, 439–445.

47 J. Mark, *Polymer Data Handbook*, N. Y. USA, 1999.

48 L. Mandelkern and R. G. Alamo, *Physical Properties of Polymers Handbook*, J. E. Mark, Springer New York, 2007.

49 L. Cai L, C. J.Foster, X. Liu, S. Wang, *Polymer*, 2014, **55**, 3836–3845.

50 L. Cai L, J. Chen, A. J. Rondinone, S. Wang, *Adv. Funct. Mater.* 2012, **22**, 3181–3190.

51 A. Favre, E. R. Fotsing and M. Levesque and E. Ruiz, *J Elastom Plast*, 2015, 1-9.

52 F. F. Estarlich, S. a Lewey, T. G. Nevell, A. a Thorpe, J. Tsibouklis and A. C. Upton, *Biofouling*, 2000, **16**, 263–275.

53 H. Zhao, D.-R. Wang, J.-W. Zha, J. Zhao and Z.-M. Dang, *J. Mater. Chem. A*, 2013, **1**, 3140.

54 S. Morlat, J.-L. Gardette, *Polymer*, 2003, **44,** 7891–7897.

55 S. Morlat and J.-C. Gardette, *Polymer*, 2001, **42**, 6071-6079.

56 F. Fraisse, S. Morlat-Thérias, J.-L. Gardette, J.-M. Nedelec, and M. Baba, *J. Phys. Chem. B* 2006, **110***,* 14678-14684.

57 Pascal De Sainte Claire, *American Chemical Society*, 2009, **42**, 3469-3482.

58 G. Gallet, B. Erlandsson, A.-C. Albertsson and S. Karlsson, *Polymer Degradation and Stability* 2002, **77,** 55–66.

59 D. F. Coker, J. R. Reimers and R. O. Watts*, Aust. J. Phys.,* 1982, **35**, 623-38.

60 M. A. Cole and C. N. Bowman, *J. Polym. Sci. Part Polym. Chem.*, 2012, **50**, 4325–4333.

61 C. P. Park, *J. Polym. Eng.*, 2001, **21**, 511-520.

62 D. Askeland, P. Fulay and W. Wright, *The Science and Engineering of Materials, SI Edition*, Cengage Learning, 2011.

63 R. Kaltseis, C. Keplinger, S. J. Adrian Koh, R. Baumgartner, Y. F. Goh, W. H. Ng, A. Kogler, A. Tröls, C. C. Foo, Z. Suo and S. Bauer, *RSC Adv.*, 2014, **4**, 27905.

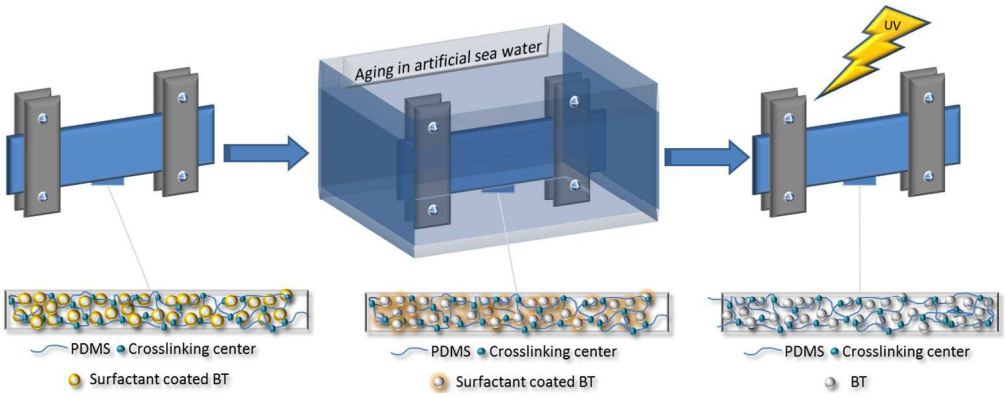


397x154mm (96 x 96 DPI)